Minimal modelling approach to describe turbulent rocket roll dynamics in a vertical wind tunnel

C E Hann, M Snowdon, A Rao, O Winn, N Wongvanich and X Chen

Proceedings of the Institution of Mechanical Engineers, Part G: Journal of Aerospace Engineering published online 21 December 2011
DOI: 10.1177/0954410011420771

Minimal modelling approach to describe turbulent rocket roll dynamics in a vertical wind tunnel

C E Hann[1]*, **M Snowdon**[1], **A Rao**[1], **O Winn**[2], **N Wongvanich**[1], and **X Chen**[2]
[1]Department of Electrical and Computer Engineering, University of Canterbury, Christchurch, New Zealand
[2]Department of Mechanical Engineering, University of Canterbury, Christchurch, New Zealand

The manuscript was received on 5 February 2011 and was accepted after revision for publication on 29 July 2011.

DOI: 10.1177/0954410011420771

Abstract: The roll dynamics of a 5-kg, 1.3 -m high sounding rocket are analysed in a vertical wind tunnel. Significant turbulence in the tunnel makes the system identification of the effective inertia, damping, and asymmetry with respect to roll challenging. A novel method is developed, which decouples the disturbance from the rocket frame's intrinsic roll dynamics and allows accurate prediction of roll rate and angle. The parameter identification method is integral-based, and treats wind disturbances as equivalent to a movement in the actuator fins. The method is robust, requires minimal computation, and gave realistic disturbance distributions reflecting the randomness of the turbulent wind flow. Two models, one with constant damping and one with fin angle-dependant damping were considered. The mean absolute roll rate of the rocket frame observed in experiments was 16.4°/s and both models predicted the roll rate with a mean absolute error less than 0.10°/s with a standard deviation less than 0.08°/s. The roll angle (measured by an encoder), was tracked by the model with a mean absolute error less than 0.20° and a standard deviation less than 0.15°. These results prove the concept of this minimal modelling approach which will be extended to varying wind speed, and pitch, and yaw dynamics in the future.

Keywords: rocketry, roll control, wind tunnel, minimal modelling, integral-based parameter identification, disturbance

1 INTRODUCTION

Sounding rockets are a fast emerging technology giving low-cost access to space [**1**]. Sounding rockets also provide important data on aerodynamics at speeds up to hypersonic [**2**], which are typically very difficult to achieve in wind tunnels [**3**, **4**]. A University of Canterbury Rocketry Research Group [**5**] has been formed to develop control systems for high accuracy positioning with a longer term goal of stabilizing rockets through the sound barrier. The idea is to use a minimal mathematical modelling approach [**6**–**9**] to describe the overall effect of complex dynamics on the inertia, damping and non-linear spring dynamics of the pitch, yaw, and roll axes of the rocket. For example, it is known that aerodynamic drag changes in each axis as a function of speed [**10**–**12**], and there are also changes in mass and inertia in each axis due to centre of mass and pressure changes over time [**10**, **13**].

The typical approach to modelling rockets is to describe motion in detail with complex 6-DOF models [**14**, **15**] and computational fluid dynamics modelling that usually requires very large computational resources and advanced testing facilities [**4**, **16**–**18**]. This article looks at the development of a simpler modelling and system identification method for understanding the roll dynamics and the effect of complex disturbances on a small spin-stabilized sounding rocket, of about 1.3 m in length and 5 kg in weight. Thus, this article concentrates on

**Corresponding author: Department of Electrical and Computer Engineering, University of Canterbury, Private Bag 4800, Christchurch, New Zealand.*
email: Chris.Hann@canterbury.ac.nz

the computational and algorithm aspects of identifying parameters from the observed data. Specifically, a methodology is created for extracting the effective torque loads from external wind variations as well as the dynamic intrinsic properties of the rocket. Thus, there is the potential for using these methods 'on-the-fly' during flight to extract the effective random forcing function due to the random wind.

The resulting modelling tool could also be used for developing and analysing various control methodologies to stabilize the rocket motion. The control mechanism considered in this research is the standard fin actuation [**19**]. Other actuation methods exist, for example gimballed thrust or attitude thrusters [**20**], but they typically require sophisticated mechanical components [**21**], so are not considered. This control development side is not a focus of this article and is left for future work.

The maximum velocity of this type of rocket is approximately 600 km/h and it can reach up to 2 km in altitude. Sounding rockets are recoverable research rockets, designed to take measurements and perform scientific experiments during flight. To simplify attitude control, this research concentrates on controlling the roll of the rocket. This approach effectively decouples the roll dynamics from the pitch and yaw avoiding complex controllers and advanced analysis [**22**].

To provide an intermediate step from simulation to a rocket launch, a vertical wind tunnel was built with a vacuum to suck air past a rocket airframe that was actuated by aluminium fins. It is important to note that the wind tunnel is not used to quantitatively identify gains for a given controller to be implemented directly on a full scale rocket launch. The overall motivation of the wind tunnel is to develop and test the system identification methodologies to allow 'smarter' rocket tests that minimize the number of launches required to stabilize a specific rocket.

There were significant disturbances in the wind tunnel due to flow separation and velocity fluctuations, which made the task of analysing the rocket's roll dynamics challenging. A typical wind tunnel is much longer and has many sections including contractions to improve the flow [**23**], for example, the Delft University [**24**] and Lund University [**25**] wind tunnels. The combination of screens and honeycomb flow straighteners is also commonly used [**26**, **27**]. The wind tunnel had none of these turbulence reducing techniques, but was sufficient to prove the concept and provided an opportunity to test algorithms on a complex system response.

System identification methods for identifying the parameters of the rocket roll response commonly involve non-linear optimization [**28**, **29**] and assume that noise and disturbance is Gaussian with zero mean [**30**]. However, it is known that for excited turbulence, which can be achieved with an active grid in a wind tunnel, the distribution of velocities is significantly non-Gaussian [**31**]. This article develops a method that can be applied to any type of random disturbance, independent of the distribution. The disturbance model is a time series of effective fin angle changes that capture the observed effects on the rocket roll velocity due to turbulent effects in the wind tunnel. The identified time series and rocket intrinsic response parameters can be used to develop a database for future control system testing. Finally, an additional goal of this article was to ensure that the methods were computationally fast and simple to implement.

2 METHODOLOGY

2.1 Experimental setup and data acquisition

To investigate spin dynamics of a small sounding rocket, a static test was performed in a vertical wind tunnel. The rocket was attached to a fixed support which allowed the rocket to roll freely about its primary axis. Control of the rocket's fins was provided by servos, which can be commanded to move to a set deflection (θ). The exact wind speed profile inside the wind tunnel was not measured, but the fan speed was held constant throughout the experiment. Figure 1 shows the setup.

In order to sense the roll position of the rocket airframe during wind tunnel testing, an optical encoder was fixed rigidly in the nose of the rocket. The rocket was then suspended on a steel rod, attached to the shaft of the optical encoder, as shown in Fig. 1. The steel rod was suspended from a cross-bar at the top of the wind tunnel such that the rod was fixed in the roll axis but allowed some movement in the pitch and yaw axes. Thus, the rocket was able to spin freely in the wind tunnel on the shaft of the optical encoder.

The optical encoder used was the Hewlett-Packard HEDS-5702-F00 quadrature [**32**], which has a resolution of 256 counts per revolution and a worst case absolute error of $\pm 5.5^\circ$ at any point in time. The encoder also has minimal starting torque ($<9.9 \times 10^{-3}$ N.m), minimal dynamic drag ($<4.9 \times 10^{-2}$ N.m) and is rated for rotation speed of up to 12 000°/s, well above the maximum rotation rates experienced in this testing. The encoder was interfaced to an ATMega8 microcontroller which relayed the position information to a laptop computer via a wireless Bluetooth link.

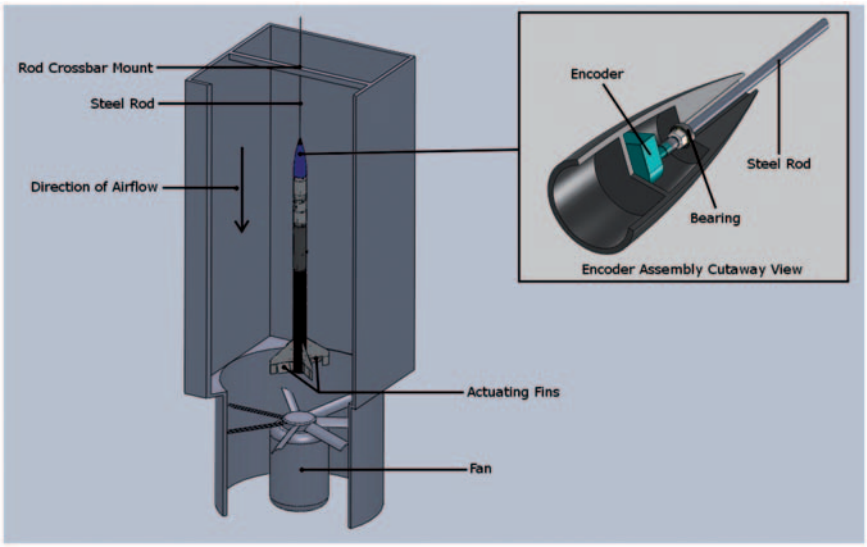

Fig. 1 Wind tunnel assembly

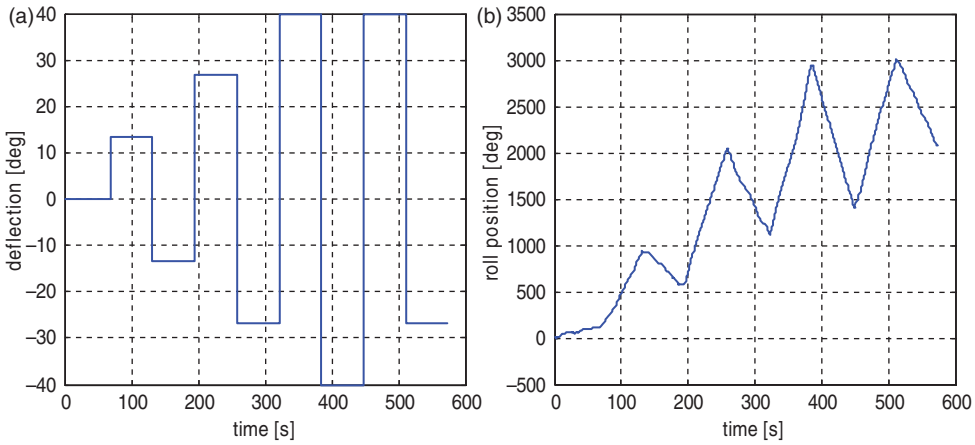

Fig. 2 (a) Input fin angle and (b) roll response

To ensure that measurements were being taken correctly, the system was 'zeroed' at a known point, then spun for several seconds before being returned to the zero point (as indicated by the system measurement). The actual alignment with the previously recorded zero point was then compared with them measured value which showed no perceivable error ($<1^\circ$).

The fins were actuated by standard RC Servos which use a 50-Hz pulse width modulation (PWM) signal to set the desired angle. The PWM signal was supplied by the on-board microcontroller, which accepted position commands from the laptop via the wireless Bluetooth link.

The fan in Fig. 1 had a maximum power of 15 kW and a maximum speed of 1445 r/min. For testing, the fan was run at 75 per cent of the maximum. Every 100 ms, both the control input and the measured roll were recorded. The control input was logged as an angle in degrees of servo deflection from the fins neutral position, while the measured roll was recorded as the angle in degrees since its initial start position which was assumed to be 0°. The data stored for analysis were taken from the time when the revolution of fan per minute had settled at 75 per cent of the maximum. Throughout the test, the roll response was recorded for several different fin positions. A significant amount of time between the transitions was provided to ensure the system was at steady state. Figure 2(a) and (b) shows the input control and output roll responses.

Once such raw data had been attained, it was then analysed by the following key steps

1. Fit a piecewise linear model to the roll step response.

2. Find a relationship between the steady-state angular velocity and fin deflection.
3. Create a bi-linear model for velocity step response that ignores external disturbances.
4. Apply integral method to identify time and torque constants.
5. Fit disturbance model to identify the disturbance present.
6. Re-simulate model with external disturbance.

Steps 1–4 involve identifying the rocket's intrinsic parameters. Since these parameters can only be determined from actuation inputs, the data considered for these steps were after the first input deflection. Steps 5 and 6 identify the external torques on the rocket when the intrinsic parameters are assumed known; hence, for these steps, all data are considered.

2.2 Modelling structure

A rigid body representation of a rocket consists of six-degree-of-freedom as shown in Fig. 3, where P, Q, and R are the roll, pitch, and yaw rates, c.g. the centre of gravity, and $\underline{\mathbf{U}}$, $\underline{\mathbf{V}}$, and $\underline{\mathbf{W}}$ the velocities in the body axes X_b, Y_b, and Z_b, respectively.

The rotational equations for the rocket in Fig. 3 are described by [**19**, **20**]

$$I_{xx}\dot{P} - QR(I_{yy} - I_{zz}) = L \tag{1}$$

$$I_{yy}\dot{Q} - PR(I_{zz} - I_{xx}) = M \tag{2}$$

$$I_{zz}\dot{R} - PQ(I_{xx} - I_{yy}) = N \tag{3}$$

where I_{xx}, I_{yy}, and I_{zz} are the rotational inertia's and L, M, and N the moments about the X_b, Y_b, and Z_b axes, respectively. A further standard simplification is to set $I_{zz} = I_{yy}$ in equation (1) due to the symmetry of the rocket [**19**, **20**]. This article concentrates on roll dynamics, since pitch and yaw controls are significantly simplified by controlling the roll [**22**]. The

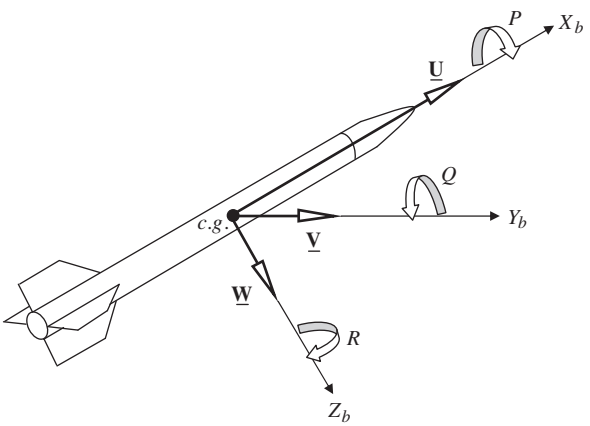

Fig. 3 Rigid body representation of a rocket

dynamics and effect of disturbances on pitch and yaw are left for future work. The roll moment L in equation (1) is defined [**19**, **20**]

$$L = q\,S\,\mathrm{d}\left[C_{beta}\beta + C_{delta}\delta + \frac{d}{2v_M}\left(C_{\dot{\beta}}\dot{\beta} + C_P P + C_R R\right)\right] \tag{4}$$

where

$$q = \frac{1}{2}\rho v_M^2 \equiv \text{dynamic pressure (kg/m s}^2\text{)} \tag{5}$$

Here, $S(\mathrm{m}^2)$ is the maximum cross-sectional area of rocket body, d(m) the maximum diameter of rocket body, $\rho(\mathrm{kg/m}^3)$ the air density, v_M the magnitude of the velocity of the centre of mass, $\beta(^\circ)$ the slide slip angle, $\delta(^\circ)$ the fin actuation angle, C_β the variation of rolling moment coefficient with angle of slide slip, C_P the variation of rolling moment coefficient with dimensionless rate of change of roll rate, $C_{\dot{\beta}}$ the variation of rolling moment coefficient with dimensionless rate of change of angle of sideslip, C_R the variation of rolling moment coefficient with dimensionless rate of change of yaw rate, and C_δ the variation of rolling moment coefficient with fin angle.

The slide slip angle (β) and rate of change ($\dot{\beta}$) terms are typically neglected [**19**]. Hence, the resulting roll dynamics can be approximated by

$$I_{xx}\dot{P} = q\,S\,\mathrm{d}\left[C_\delta\delta + \frac{d}{2v_M}(C_P P + C_R R)\right] \tag{6}$$

In general, the yaw-roll coupling in equation (6) is weak [**33**]; hence, for this article, the yaw contribution to roll moment is ignored. The main cases where yaw–roll coupling can be significant are for the lateral modes known as inertial roll and spiral divergence [**34**–**36**].

The inertial roll [**34**, **35**] is caused by fast roll rates which can significantly affect pitch and yaw as shown in equations (2) and (3). These effects also result in significant side slip, which have caused structural failure on the tails of several aircraft [**35**]. Appropriate design of the tail [**35**] can help mitigate this instability as well as minimizing the roll rate. Spiral divergence, consisting of an ever increasing roll angle, coupled with the yaw angle. For aircraft, the flight path is a slowly steepening coordinated turn. This lateral mode is very slow and easily compensated [**36**]. Note that, wind turbulence may also increase the yaw rate rapidly as well as the sideslip angle β and rate $\dot{\beta}$ in equation (4), which would affect the dynamics of roll in equation (1). However, for this article, all external disturbances affecting roll are lumped into a generic disturbance profile.

After simplifying some notation, the resulting model is defined

$$I\dot{v} = -cv + b\theta + \tau_d(t) \tag{7}$$

where

$$I = I_{xx} \equiv \text{rotational inertia},\ v = p \equiv \text{rollvelocity},$$
$$c = \frac{q\,S\,d^2|C_P|}{2v_M}\ b = q\,S\,d\,C_\delta,\ \theta = \delta \equiv \text{fin angle},$$
$$\tau_d(t) \equiv \text{external disturbance torque affecting roll} \tag{8}$$

The parameters c and b in equations (7) and (8) are considered as the overall effective roll damping and torque constants that convert a fin angle into a torque about the roll axis.

In the case of the wind tunnel experiment of Fig. 1, the velocity v_M and the density ρ can be considered to be constant over time. The effect of turbulence in the wind tunnel is to give a disturbance on the intrinsic response of the rocket to a fin angle change. In other words, the turbulence is represented by a time-varying external disturbance torque $\tau_d(t)$ in equation (8).

2.3 Piecewise linear approximation to the roll step response

The roll response of the rocket airframe is close to piecewise linear, as shown in Fig. 2(b). Thus, as an initial approximation, a piecewise linear model with eight steps was formulated for θ

$$\begin{aligned}\theta_{model}(t) &= a_1 + b_1\,t, \quad T_1 \le t < T_2 o\\ &\vdots\\ &= a_8 + b_8\,t, \quad T_8 \le t < T_{end}\end{aligned} \tag{9}$$

with equality constraints

$$a_i + b_i T_{i+1} = a_{i+1} + b_{i+1} T_{i+1}, \quad i = 1, \ldots, 7 \tag{10}$$

Let N_i be the number of time points in each ith segment $t \in [T_i,\ T_{i+1})$ of equation (9) at the sampling frequency of 10 Hz, and define

$$\boldsymbol{T}_{vector} = \left[t_1, t_2, \ldots, t_{\bar{N}}\right), \quad \bar{N} = N_1 + \cdots + N_8 \tag{11}$$

For ease of notation, define $N_0 = 0$, denote the measured data as $\theta_{data}(t)$, and define

$$\bar{\boldsymbol{T}}_{N_{i\times 2}} = \begin{pmatrix} 1 & t_{N_{i-1}+1} \\ \vdots & \vdots \\ 1 & t_{N_i} \end{pmatrix}, \quad i = 1, \ldots, 8 \tag{12}$$

$$\underline{\boldsymbol{O}}_{m\times n} \equiv m \times n \text{ matrix of zeros} \tag{13}$$

Setting $\theta_{model}(t) = \theta_{data}(t)$ for $t \in \boldsymbol{T}_{vector}$ of equation (11) gives a set of $\bar{N}$ equations in 16 unknowns $\{a_1,\ b_1, \ldots, a_8,\ b_8\}$, which can be written in the form

$$\boldsymbol{AX} = \boldsymbol{B} \tag{14}$$

$$\boldsymbol{A} = \begin{pmatrix} \bar{\boldsymbol{T}}_{N_1\times 2} & \underline{\boldsymbol{O}}_{N_1\times 2} & \cdots & \underline{\boldsymbol{O}}_{N_1\times 2} \\ \underline{\boldsymbol{O}}_{N_2\times 2} & \bar{\boldsymbol{T}}_{N_2\times 2} & \cdots & \underline{\boldsymbol{O}}_{N_2\times 2} \\ \vdots & \vdots & \ddots & \vdots \\ \underline{\boldsymbol{O}}_{N_8\times 2} & \underline{\boldsymbol{O}}_{N_8\times 2} & \cdots & \bar{\boldsymbol{T}}_{N_8\times 2} \end{pmatrix},$$
$$\boldsymbol{B} = \begin{pmatrix} \theta_{data}(t_1) \\ \vdots \\ \theta_{data}\left(t_{\bar{N}}\right) \end{pmatrix} \tag{15}$$

Equation (14) is solved by linear least squares with the equality constraints of equation (10) to determine the best fit of the model of equation (9) to the measured roll data of Fig. 2(b). Matlab was used for all calculations. The result is given in Fig. 4.

2.4 Correlating the steady-state angular velocity and fin deflection

The stepwise approach of Fig. 2(a) allows the steady-state dynamics of the fin deflection to roll rate to be simply modelled. Eight step inputs of various magnitudes were carried out in the experiment, as shown in Fig. 2(a). The slopes $\{b_1, \ldots, b_8\}$ in Fig. 4 determine eight steady-state values of the roll rate v_{ss} corresponding to each steady-state fin deflection (f_{ss}) of Fig. 2(a). The values of f_{ss} and v_{ss} are plotted in Fig. 5 with a linear best fit

$$v_{ss,new} = \alpha f_{ss} + \beta \tag{16}$$

$$\alpha = 0.6590, \quad \beta = 2.8856 \tag{17}$$

The correlation coefficient of $R^2 = 0.9914$ shows that there is a very strong linear relationship.

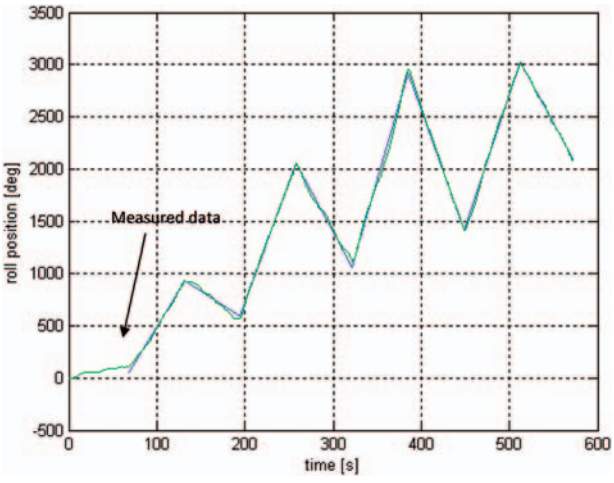

Fig. 4 Piecewise linear model of the roll response to the eight step changes in Fig. 2(a)

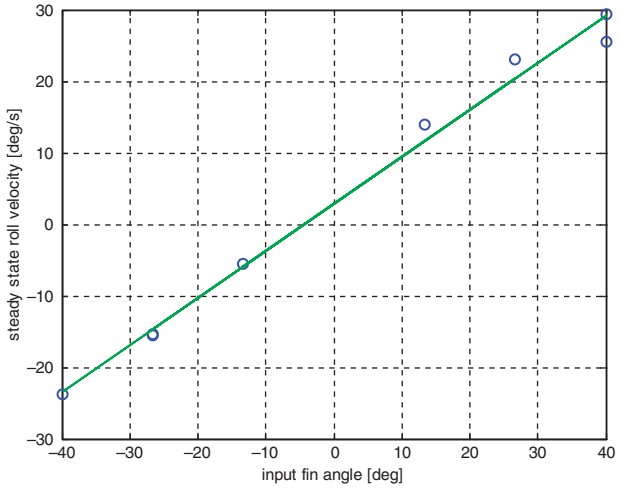

Fig. 5 Correlation between steady-state deflection and roll rate with the best fit line of equations (16) and (17)

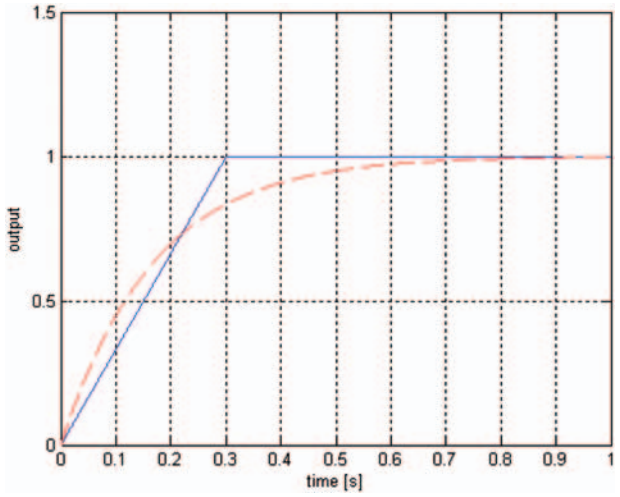

Fig. 6 Bi-linear approximation (solid blue line) to an over damped response modelled by an ordinary differential equation (dashed red line)

2.5 Bi-linear modelling of velocity step response

The roll dynamics of rockets are well known to be over damped [**10**, **11**, **13**] and thus they can be modelled as a first-order differential equation [**10**]. The solution to a step response of a first-order system can be approximated as a bi-linear model, as shown in Fig. 6. The general form of a bi-linear model is defined

$$v_{model} = \begin{cases} \frac{v_{ss}-v_0}{t_0}\, t + v_0, & 0 < t < t_0 \\ v_{ss}, & t > t_0 \end{cases} \tag{18}$$

where it is assumed that v_{ss} and v_0 are known and t_0 is unknown. The velocity step response, which the model of equation (18) approximates, is computed by differentiating the roll angle data in Fig. 2(b).

The values of v_{ss} at each velocity step are determined from the corresponding input deflection f_{ss} using the linear model of equation (16). This approach ensures that the model predicted v_{ss} is anti-symmetric about the point of $v_{ss} = 0$, and essentially acts as a model-based filter on the external disturbances to obtain a consistent model of the intrinsic rocket roll steady-state response. Values of v_0 are taken to be the previous value of v_{ss}.

The break point t_0 in equation (18) is assumed to lie less than a given amount ΔT_0 after the initial time point. For this experiment, ΔT_0 was empirically chosen to be 4 s to minimize the search space, but it is essentially arbitrary. The approach used to identify t_0 is to increment from 0 to 4 s in steps of 0.01 s, and compute the least square error between the model of equation (18) and the interpolated measured data. Figure 7(a) shows the least square error plotted *versus* the position of the breakpoint for the 8th velocity step response. The value of t_0 chosen in this case was 1.61 s which corresponds to the lowest error and the best fit of the bi-linear model to the data.

Figure 7(b) plots the approximated velocity (blue dotted line) using equation (18) *versus* the true velocity (green solid line). This result shows that the model of equation (18) is sufficient to capture the overall steady-state response even though there is a lot of external disturbance present in the raw velocity readings. This disturbance is not sensor error, but is a real effect coming from turbulence in the wind tunnel [**1–3**, **22**, **23**].

2.6 Modelling and integral-based parameter identification – intrinsic rocket parameters

The bi-linear approximation shown in Fig. 7(b) effectively removes the disturbance from the data. In other words, this reconstructed velocity can be modelled with the assumption that roll dynamics are only affected by the inputs to the servo motors and there is no external disturbance. Therefore, the rocket's roll dynamics can be described by

$$I\dot{v} = -cv + f_{ext}(\theta) \tag{19}$$

where I is the rotational inertia, c the damping parameter, and $f_{ext}(\theta)$ the external torque resulting from a change in the fin angle θ.

Consider the following formulation of equation (19)

$$I\dot{v} = -c(v - (\alpha\theta + \beta)) \tag{20}$$

At each steady-state $\theta = \theta_{ss}$ with $\dot{v} = 0$, $v = \alpha\theta_{ss} + \beta = v_{ss}$ in equation (20). Hence, the model of equation (20) contains implicitly the linearized steady-state model of equation (16). Equating equation (20) with

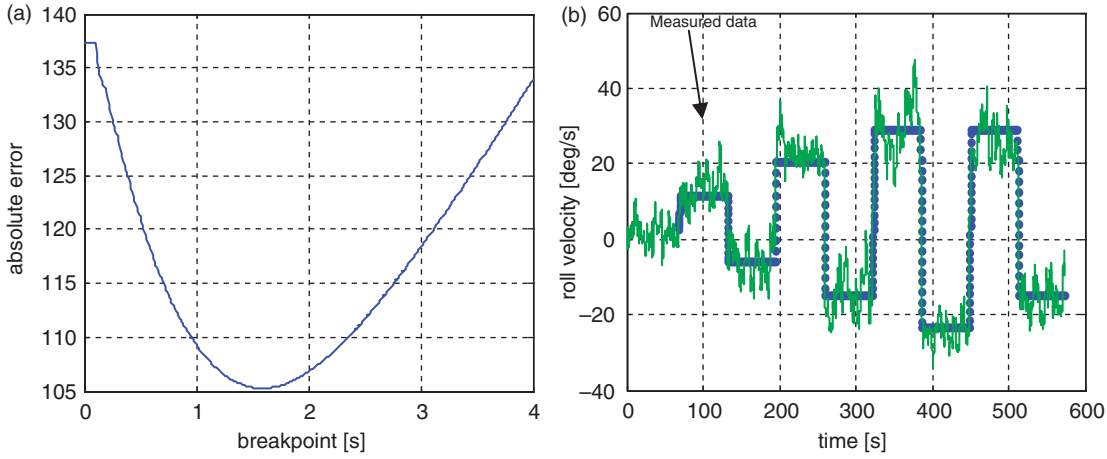

Fig. 7 (a) Error between model and data while varying the break point. (b) Bi-linear approximation velocity step response

equation (19) shows that $f_{ext}(\theta) = c(\alpha\theta + \beta)$. Both parameters, I and c, cannot be individually identified from the roll velocity alone. Thus, the model of equation (20) is rewritten in the form

$$\dot{v} = -a(v - (\alpha\theta + \beta)) \tag{21}$$

where

$$a = \frac{c}{I} \tag{22}$$

Equations (21) and (22) lump the two parameters I and c into a generic damping parameter a.

2.6.1 Fin angle (θ) dynamics

In the servo motors, there is a time lag between the commanded fin position and the actual steady-state fin position. This time lag has been measured to be 0.4 s for a 60° fin angle change. A general formula taking this effect into account is defined

$$t_{lag} = \left|\theta_{data}(t_{N+1}) - \theta_{data}(t_N)\right| \times \frac{0.4}{60} \tag{23}$$

For example, given the second step input from 13.3° to −13.3° in Fig. 2(a), the time taken for the fin angle to reach steady state is

$$\begin{aligned} t_{lag} &= |-13.3 - 13.3| \times \frac{0.4}{60} \\ &= 0.17\,\text{s} \end{aligned} \tag{24}$$

The time-varying response of the fin angle calculated using equation (24) is shown in Fig. 8.

The model of equation (21) relates the angular acceleration to the rocket's current angular velocity (v) and current fin deflection (θ). The variable a, which is the inverse of the time constant, is therefore the unknown parameter, and the precise value of the rotational inertia I is not required.

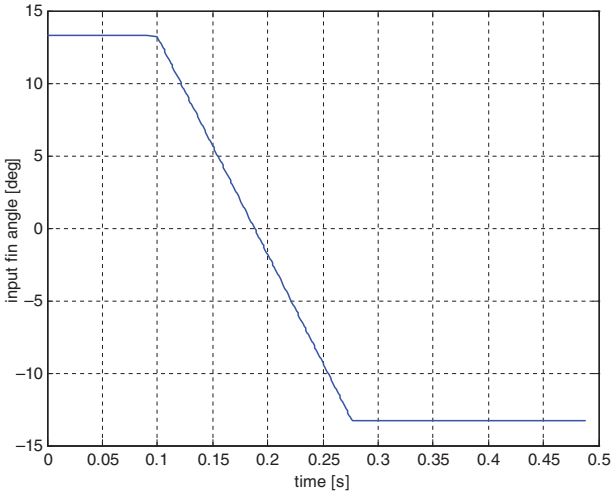

Fig. 8 Approximation to fin angle due to time delay in servo motors

2.6.2 Constant damping parameter

It is first assumed that the unknown parameter a in equation (21) is constant for all times. To identify a, an integral-based method similar to [**37**, **38**] is formulated. Equation (21) is first integrated over each input step period, which yields

$$\begin{aligned} v(t) &= v(T_1) - a\int_{T_1}^{t}(v - (\alpha\theta + \beta))\mathrm{d}t, \quad T_1 \le t < T_2 \\ &\vdots \\ &= v(T_8) - a\int_{T_8}^{t}(v - (\alpha\theta + \beta))\mathrm{d}t, \quad T_8 \le t < T_{end} \end{aligned} \tag{25}$$

Denote the measured velocity as $v_{data}(t)$. Equating $v(t)$ of equation (25) with $v_{data}(t)$ for $t \in \boldsymbol{T}_{vector}$ of equation (11) gives a set of $\bar{N}$ equations in the one

unknown parameter a. These equations are defined by the matrix equation

$$\begin{pmatrix} \boldsymbol{I}_{N_1} \\ \vdots \\ \boldsymbol{I}_{N_8} \end{pmatrix} a = \begin{pmatrix} \bar{\boldsymbol{v}}_{data,\,N_1} \\ \vdots \\ \bar{\boldsymbol{v}}_{data,\,N_8} \end{pmatrix} \tag{26}$$

where

$$\bar{\boldsymbol{v}}_{data,\,N_i} = \begin{pmatrix} v_{data}(T_i + \Delta t) - v_{data}(T_i) \\ \vdots \\ v_{data}(T_i + N_i \Delta t) - v_{data}(T_i) \end{pmatrix} \tag{27}$$

$$\mathrm{I}_{N_i} = -\Big[\int_{T_i}^{T_i+\Delta t} (v - (\alpha\theta + \beta))\mathrm{d}t, \ldots, \int_{T_i}^{T_i+N_i\Delta t} (v - (\alpha\theta + \beta))\mathrm{d}t \Big]^T, \quad i = 1, \ldots, 8 \tag{28}$$

The integrals in equation (28) are numerically evaluated using the trapezium rule, and the parameter a is found by solving equation (26) by linear least squares.

Equation (21) can be written in the form

$$\dot{v} = -av + b\big(\theta + \bar{\theta}\big) \tag{29}$$

where

$$b = a\alpha, \quad \bar{\theta} = \beta/\alpha \tag{30}$$

The quantity $b\bar{\theta}$ in equation (29) represents the torque offset that occurs due to asymmetries across the rocket's primary axis. In other words, with no fin angle ($\theta = 0$) the rocket will still spin. The parameter $\bar{\theta}$ can be interpreted as the equivalent fin angle that would reproduce this spin if the rocket was perfectly symmetric. The parameter b is the torque constant that relates a movement in the fin angle to an applied torque on the rocket.

2.6.3 Time-varying damping parameter

The unknown parameter a in equation (21) is next assumed to vary across each step change of Fig. 2(a). Specifically, $a(t)$ is defined by

$$\begin{aligned} a(t) &= a_1, \quad T_1 \le t < T_2 \\ &\vdots \\ &= a_8, \quad T_8 \le t < T_{end} \end{aligned} \tag{31}$$

This assumption can reveal if the intrinsic parameters of inertia and damping of the rocket are significantly altered by fin actuation, and whether there is any clear trend. It is an example of the overall concept of this research which is to describe complexity by interactions of simpler models [**6**–**9**] rather than one highly detailed and computationally intensive model.

The method for identifying a time-varying parameter a follows a similar approach to equations (25) to (27). An integral formulation of equation (21) is defined by

$$\begin{aligned} v(t) &= v(T_1) - a_1 \int_t^{T_1} (v - (\alpha\theta + \beta))\mathrm{d}t, \quad T_1 \le t < T_2 \\ &\vdots \\ &= v(T_8) - a_8 \int_t^{T_8} (v - (\alpha\theta + \beta))\mathrm{d}t, \quad T_8 \le t < T_{end} \end{aligned} \tag{32}$$

where

$$\mathrm{C} \begin{pmatrix} a_1 \\ \vdots \\ a_8 \end{pmatrix} = \bar{\boldsymbol{v}}_{data} \tag{33}$$

$$\mathrm{C} = \begin{pmatrix} \boldsymbol{I}_{N_1} & \underline{\boldsymbol{O}}_{N_1\times 1} & \cdots \underline{\boldsymbol{O}}_{N_1\times 1} \\ \underline{\boldsymbol{O}}_{N_2\times 1} & \boldsymbol{I}_{N_2} & \cdots \underline{\boldsymbol{O}}_{N_2\times 1} \\ \vdots & \ddots & \vdots \\ \underline{\boldsymbol{O}}_{N_8\times 1} & \underline{\boldsymbol{O}}_{N_8\times 1} & \cdots \boldsymbol{I}_{N_8} \end{pmatrix} \tag{34}$$

and $\bar{\boldsymbol{v}}_{data}$ and $\boldsymbol{I}_{N_i}$ are given in equation (27). Hence, the linear least square solution of equation (33) defines the best fit of the model of equation (32) to the measured data, $\bar{\boldsymbol{v}}_{data}$.

2.7 Modelling system disturbance

There are significant turbulent flows and velocity fluctuations present in the wind tunnel of Fig. 1. Turbulent flow models are common in literature but they are usually very computationally intensive and require many parameters to identify or estimate [**39**, **40**].

The approach of this article is to capture the complex flow disturbances by computing the effective applied torque on the rocket at discrete intervals. The applied torque is modelled as the fin angle change needed to reproduce the observed roll dynamics in a theoretically laminar steady flow. Mathematically the model is defined by the reformulation of equation (29)

$$\dot{v} = -av + b(\theta + \bar{\theta} + u_d) \tag{35}$$

where u_d is the unknown time-varying disturbance due to turbulence in the wind tunnel, and a, b, and $\bar{\theta}$ are defined in equation (30).

To reflect the fact that a is changing for different fin angles in equation (30), for generality equation (35) is written in the following form

$$\dot{v}(t) = -a(t)\big(v(t) - \alpha\big(\theta(t) + \bar{\theta} + u_d(t)\big)\big) \tag{36}$$

where α and $\bar{\theta}$ are constants. Equation (36) follows from substituting $b = a(t)\alpha$ from equation (30) into equation (35) and factoring for $a(t)$.

2.7.1 Identifying $u_d(t)$

The parameters $a(t)$, $v(t)$, $\theta(t)$, α, and $\bar{\theta}$ in equation (36) are assumed known, and the unknown disturbance profile $u_d(t)$ is taken to be a piecewise constant function over intervals of length Δt which is chosen empirically. For the experiment, the measurements were logged every 0.1 s; thus, Δt is chosen to be 0.1 s.

Let N_{total} be the number of time intervals Δt that fit in the whole time period on the experiment, and denote $\bar{v}_{data}(t)$ as the measured data interpolated at the frequency of 100 Hz, or equivalently with the sampling period of $\delta t = 0.01$ s. Let

$$t_i = i\Delta t, \qquad i = 1, \ldots, , N_{\text{total}} \tag{37}$$

Integrating equation (36) from t_{i-1} to t yields

$$v(t_i) - v(t_{i-1}) = -a(t_{i-1}) \int_{t_{i-1}}^{t} \big(v(t) - \alpha\big(\theta(t) + \bar{\theta}\big)\big)\mathrm{d}t + \bar{u}_{\mathrm{d},i}(t - t_{i-1}), \quad t_{i-1} \le t < t_i \tag{38}$$

$$\bar{u}_{\mathrm{d},i} = a(t_{i-1})u_{\mathrm{d},i} \tag{39}$$

where $u_{d,i}$ is an unknown constant across the time interval $[t_{i-1}, t_i)$of length Δt, and $a(t) = a(t_{i-1})$ is constant in this interval, since it is defined by equation (31). Choosing time points in each interval $t_{i-1} \le t < t_i$ at the sampling period of δt yields a vector

$$\bar{\boldsymbol{t}}_{vector,i} = \{t_{i-1} + \delta t,\ t_{i-1} + 2\delta t, \ldots, , \ t_{i-1} + \Delta t\} \tag{40}$$

of length

$$N_t = 100\delta t = 100 \times 0.1 = 10 \tag{41}$$

Substituting $N_t = 10$ values of $t \in \bar{t}_{vector}$ in equation (40) into equation (38) gives ten equations in one unknown $\bar{u}_{\mathrm{d},i}$ which can be written in matrix form

$$\bar{C}_i \bar{u}_{\mathrm{d},i} = \bar{D}_i \tag{42}$$

$$\bar{C}_i = \begin{pmatrix} \delta t \\ 2\delta t \\ \vdots \\ N_t\delta t \end{pmatrix},$$

$$\bar{D}_i = \begin{pmatrix} v(t_{i-1} + \delta t) - v(t_{i-1}) + a(t_{i-1}) \int_{t_{i-1}}^{t_{i-1}+\delta t} \big(v(t) - \alpha\big(\theta(t) + \bar{\theta}\big)\big)\mathrm{d}t \\ \vdots \\ v(t_{i-1} + N_t\delta t) - v(t_{i-1}) + a(t_{i-1}) \int_{t_{i-1}}^{t_{i-1}+N_t\delta t} \big(v(t) - \alpha\big(\theta(t) + \bar{\theta}\big)\big)\mathrm{d}t \end{pmatrix} \tag{43}$$

For each $i = 1, \ldots, , N_{\text{total}}$, equation (42) can be solved by linear least squares to find the unknown constant $\bar{u}_{\mathrm{d},i}$. Once $\bar{u}_{\mathrm{d},i}$ is computed, the disturbance value $u_{\mathrm{d},i}$can be determined from equation (39). The final result is a piecewise constant function

$$u_d(t) = \sum_{i=1}^{N_{\text{total}}} (H(t - t_{i-1}) - H(t - t_i))u_{\mathrm{d},i} \tag{44}$$

$$\begin{aligned} H(t) &= 1, \quad t > 0 \\ &= 0, \quad t < 0 \end{aligned} \tag{45}$$

where $H(t)$ is the standard Heaviside function and $u_d(t)$ describes the disturbance profile, or set of fin angle changes, that provides the best model fit of equation (36) to the measured data $\bar{v}_{data}(t)$.

2.8 Summary of algorithm

Figure. 9 gives a summary of the algorithm used to determine the intrinsic rocket roll parameters.

3 RESULTS AND DISCUSSION

3.1 Identification of intrinsic rocket roll parameters

The rocket roll intrinsic parameters are given by a, b, and $\bar{\theta}$ as defined in equations (29) and (30), without any disturbance. The parameter a, which determines b, is either constant or can vary across each step change of the fin angle in Fig. 2(a).

3.1.1 Constant parameter

For a constant parameter a in equations (29) and (30), applying steps 1–4 in the algorithm of Fig. 9 yields

$$a = 1.314\,\mathrm{s}^{-1}, \quad b = 0.8665\,\mathrm{s}^{-2}, \quad \bar{\theta} = 4.38^{\circ} \tag{46}$$

These parameters give the best least square fit of the model of equation (29) to the bi-linear approximated velocity step response in Fig. 7(b). Figure 10 plots an overlay of the modelled response *versus* this bi-linear approximated response.

To see the transient response more clearly, Fig. 11 plots a close-up version of the increasing transient and the decreasing transient associated with the fin angle changes from the fourth to sixth periods. As is expected, the model precisely captures the steady state and also captures quite closely the transient responses.

3.1.2 Time-varying parameter

For a time-varying parameter $a = a(t)$ in equations (29) and (30), steps 1–4 in Fig. 9 give a sequence of eight values of a and b shown in Table 1. The value of $\bar{\theta}$ is the same as that given in equation (46).

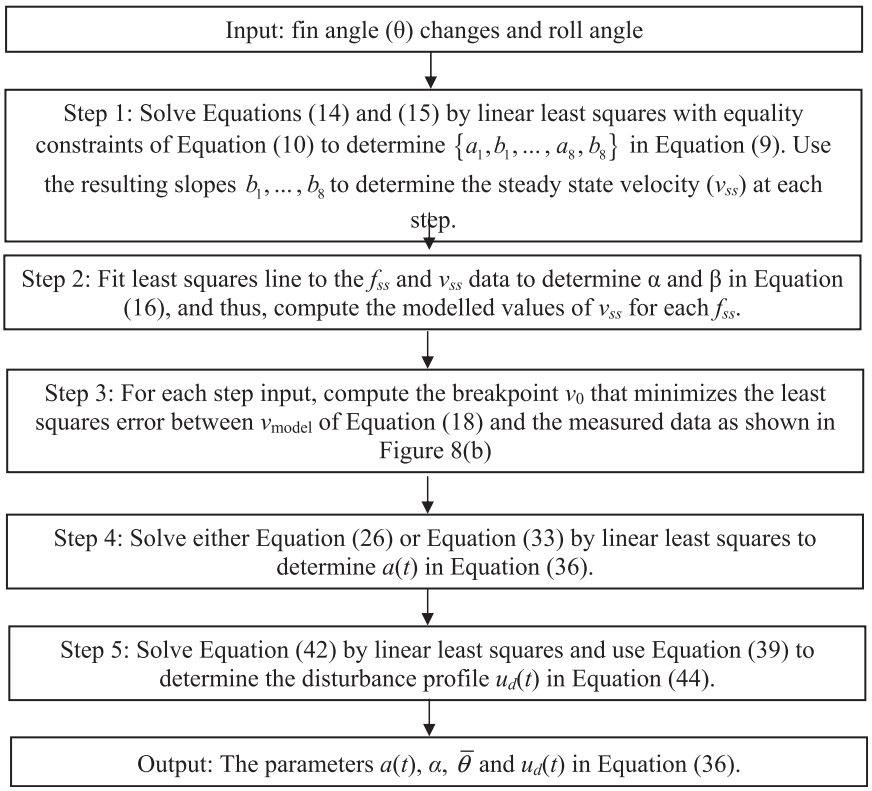

Fig. 9 Algorithm to determine intrinsic rocket roll parameters $a(t)$, α, and $\bar{\theta}$ and external disturbance profile $u_d(t)$ in equation (36)

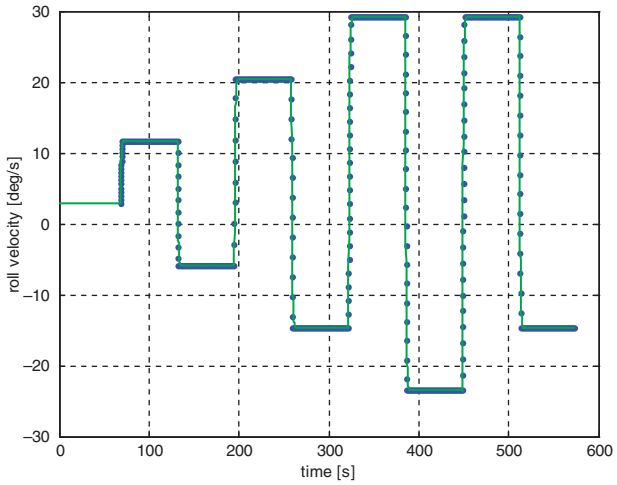

Fig. 10 Bi-linear approximation to velocity (blue dotted line) compared with velocity approximation (green solid line) with constant damping coefficient

For Table 1, the parameter a is assumed to be piecewise constant over each time period. The method of equations (30) identifies a different a independent of the fin angle. For example, the 5th and 7th values of a are slightly different even though the fin angles are both 40°. This approach ensures complete freedom is allowed in the solution to reveal trends without any presumptions on dynamics.

To simplify notation, define

$$\theta_{\text{effective}} = \theta + \bar{\theta} \tag{47}$$

which is the sum given in the model of equation (29). Equation (47) implies that to obtain zero torque from the input fin angle, an angle of $\theta = -\bar{\theta} = -4.38^\circ$ on the rocket is required.

Figure 12 plots the damping values a in Table 1 *versus* the absolute value of this adjusted fin angle $\theta_{effective}$ to account for the asymmetry of the rocket. Thus, the quantity $|\theta_{effective}|$ assumes symmetry about $\theta = -\bar{\theta}$. With the omission of the clear outlier, there is a strong negative correlation with $R^2 = 0.8280$ in Fig. 12. The reason for the outlier is likely due to an increased amount if disturbance present just at the point where the fin angle changes, as shown in Fig. 13.

The result of Fig. 12 suggests that the damping coefficient a decreases as $|\theta_{effective}|$ increases. In other words, the rocket roll takes longer to reach steady state from a given starting point of a large fin angle compared to a starting point of a small fin angle. This behaviour can be explained by an increase in inertia as the fins go outwards, since the inertia is on the denominator of equation (22).

Physically, as the fins go outwards there is an added mass due to a greater mass of air being moved by the

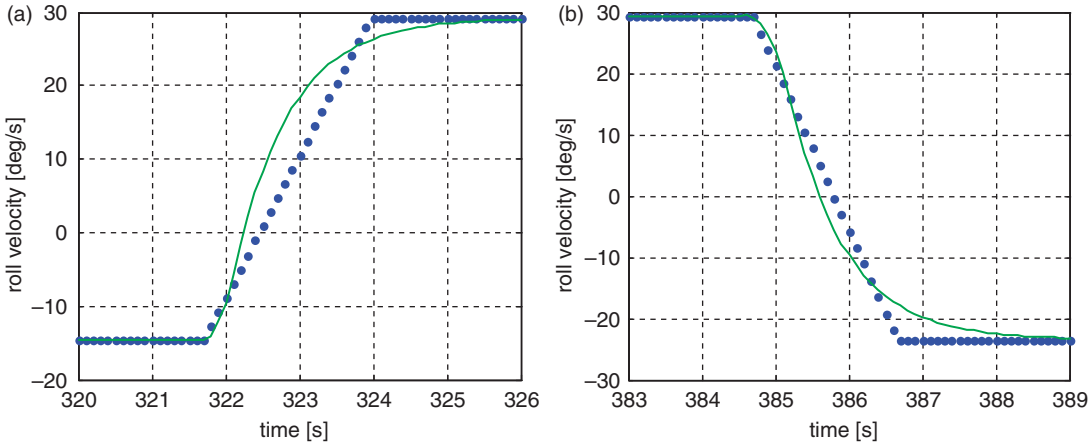

Fig. 11 Close-up views of (a) fifth step input in Fig. 10 and (b) sixth step input in Fig. 10

Table 1 Time-varying intrinsic parameters a and b from equations (29) and (30)

Time period (s)	Fin angle (°)	a (s^{-1})	b (s^{-2})
[68.1,131.4)	13.33	1.6876	1.1121
[131.4,194.7)	−13.33	2.2831	1.5046
[194.7,258.2)	26.67	3.2439	2.1377
[258.2,321.7)	−26.67	2.2208	1.4635
[321.7,384.7)	40.00	1.1011	0.7256
[384.7,448.3)	−40.00	1.4018	0.9238
[448.3,511.6)	40.00	1.0997	0.7247
[511.6,573.0)	−26.67	1.7653	1.1633

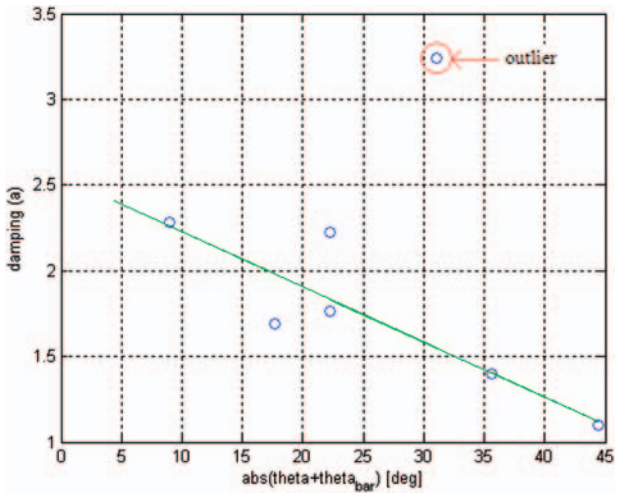

Fig. 12 Plot of the absolute effective fin angle, $|\theta_{effective}|$, *vs* damping co-efficient denoted by circles. The best fit line, ignoring the outlier, is also shown

rocket's air frame. The concept of 'added mass' is well known in boat dynamics where the apparent mass increases, e.g. response in the yaw axis is effectively greater than the actual measured mass of the boat [**41**]. Thus, a rocket rotating at a constant speed with a large fin angle will have a greater effective rotational inertia than that rotating with a small fin angle.

The linear relationship in Fig. 12 is described by

$$a(\theta) = \bar{\alpha}\left|\theta + \bar{\theta}\right| + \bar{\beta}, \quad \bar{\alpha} = -0.0289, \quad \bar{\beta} = 2.4075 \tag{48}$$

Replacing a in equations (29) and (30) with $a(\theta)$ in equation (48) and factorizing give an extended nonlinear model of the roll dynamics

$$\dot{v} = -a(\theta)\left(v - \alpha\left(\theta + \bar{\theta}\right)\right) \tag{49}$$

This model of equation (49) is an example of the philosophy of this research where more complex models can be created from simplified model structures as required to capture measured data and observed trends. Of course, more experiments, and ultimately rocket launches, will be required to fully validate the accuracy of the model of equation (49), but it shows the concept. The parameter $a(t)$ in equation (29) will also change as a function of the rocket speed or Mach number [**10**, **11**], but these cases are left for future work.

3.2 Identification of external disturbance *ud(t)* on rocket roll dynamics

The rocket roll response with external disturbances present is modelled by equation (36) where the parameters $a(t)$, α, and $\bar{\theta}$are assumed to be known, and $v(t)$ and $\theta(t)$ are directly measured. The value of the parameter a is either constant as given in equation (46) or a function of fin angle as given in equation (48), which gives two possible $u_d(t)$ profiles. For the purposes of analysis and discussion, define

$$u_{\mathrm{d},constant}(t) \equiv \text{identified disturbance based on}\} \text{constant damping coefficient of equation (46)} \tag{50}$$

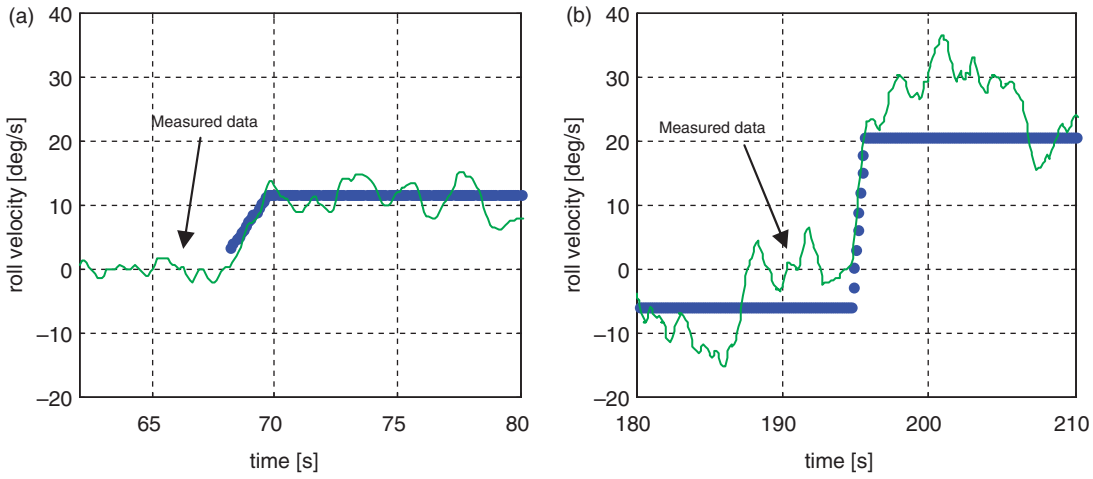

Fig. 13 (a) Close-up of first period of fin angle change with relatively small disturbance. (b) Close-up of third period of fin angle change with large disturbance

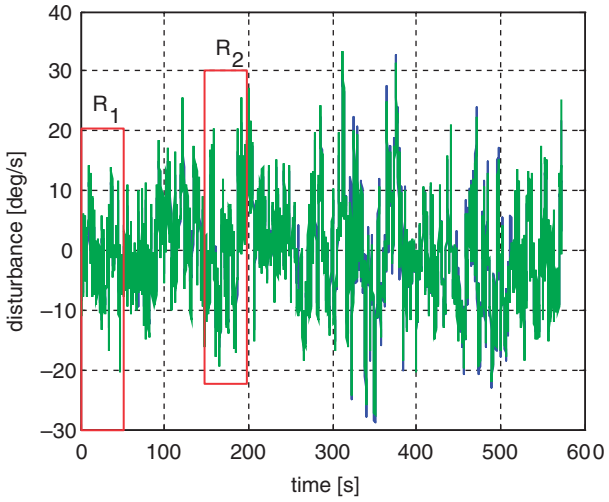

Fig. 14 Identified disturbance based on $u_{d,constant}(t)$ of equation (50) (dotted green line) and $u_{d,\theta}(t)$ of equation (51) (solid blue line)

$$u_{\mathrm{d},\theta}(t) \equiv \text{identified disturbance based on } \theta\text{−dependant damping coefficient } a(\theta) \text{ in equations (48) and (49)} \tag{51}$$

Figure 14 shows the result of applying step 5 of the algorithm in Fig. 9 for both cases. Note that a three-point moving average is applied several times to the velocity in Fig. 7(b) to smooth out noise. Figure 15 shows two close-up regions R_1 and R_2 of Fig. 14 for more clarity. Although the two disturbances are quite close and follow the same trend, the disturbance $u_{d,\theta}$ has, in general, less pronounced peaks and undershoots the disturbance $u_{d,constant}$. Specifically, the 90 per cent confidence intervals of $u_{d,\theta}(t)$ and $u_{d,constant}(t)$ are [−13.38, 14.28] and [−14.07, 15.15], respectively.

This result shows that for the $u_{d,constant}$ case, the algorithm 'lumps' the error in the constant damping coefficient a into the disturbance profile, so that sharper changes occur. A 'smoother' profile of $u_{d,\theta}$ suggests that the model of equation (49) is potentially better than the model of equation (29) which has constant parameters. However, although the modelling technique may give a more physically accurate description of rocket roll dynamics; further wind tunnel tests and rocket launches are required to fully validate whether there is any significant practical gain in using the more complex model of equation (49).

3.3 Error analysis

In a rocket flight, a rate gyro would be used to measure the roll velocity in Fig. 7(b), which has potentially greater noise than an encoder. To test the effects of noise on the sensor, 100 Monte Carlo simulations were done at four different noise levels 1 per cent, 2 per cent, 5 per cent, and 10 per cent for the constant damping coefficient case of equation (50). The noise model for the velocity data is defined (Fig. 16)

$$v_{noise} = \left(1 + \frac{\eta}{100}\varepsilon\right) v_{data}, \qquad \eta = 0,\ 1,\ 2,\ 5,\ 10,$$
$$\varepsilon \equiv \text{random number from normal distribution,}$$
$$\mu = 0, \sigma = 1 \tag{52}$$

Data were sampled at 100 Hz, and Fig. 14 shows an example of the noise-corrupted roll velocity data *versus* the measured roll velocity data from the encoder for 10 per cent noise.

The method of Fig. 9 is applied on the noise-corrupted roll velocity data, and Fig. 17 shows the 90th

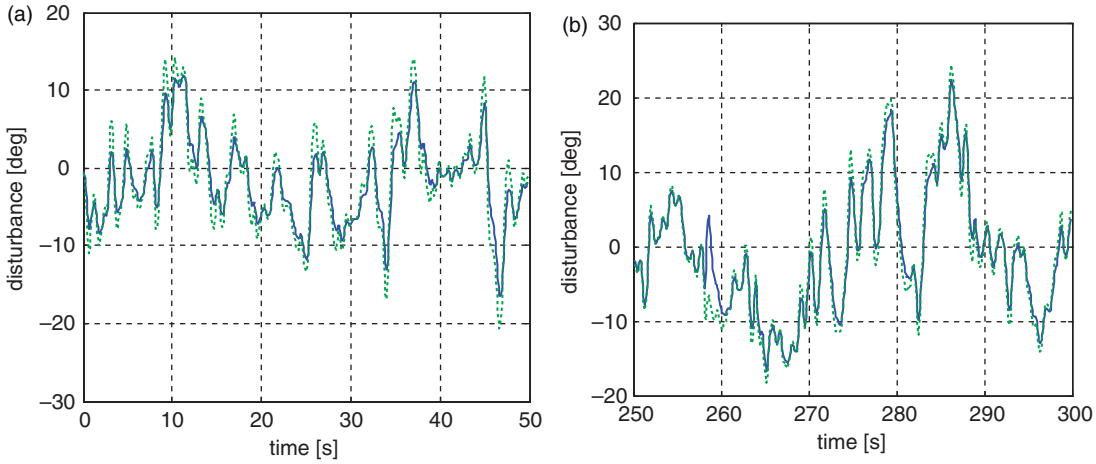

Fig. 15 Close-up regions: (a) R_1 and (b) R_2 in Fig. 14

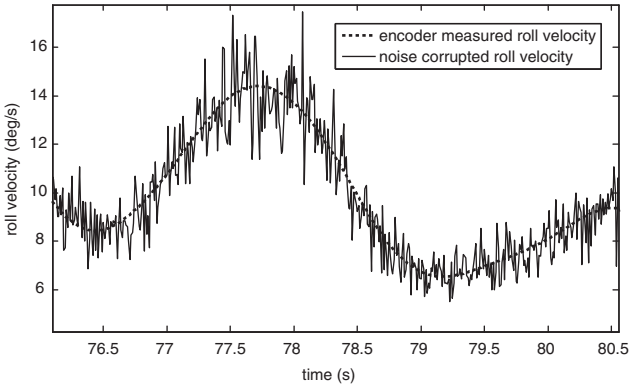

Fig. 16 Adding 10 per cent noise to the roll velocity using the model of equation (52)

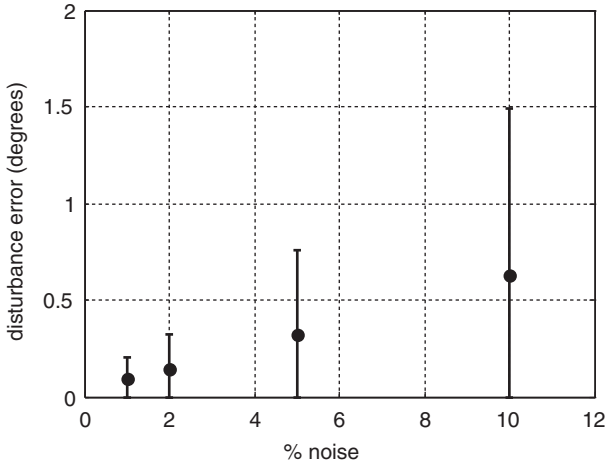

Fig. 17 The mean absolute error and 90th percentile errors *vs* noise level

percentile absolute errors in the identified disturbance *versus* the noise level. The noise increases linearly, and for 10 per cent noise, the mean absolute error is 0.62° with a 90th percentile of 1.49°. Thus, for noise levels up to 10 per cent, and a sampling frequency of 100 Hz, the mean absolute errors in the identified disturbance are less than 2 per cent of the maximum disturbance angle of 32° in Fig. 14. One of the main reasons for this robustness to noise is that the method depends on integrals of the measurements, which effectively smooth the data.

3.4 External disturbance distributions

The normalized histograms of the disturbances $u_{d,\theta}(t)$ and $u_{d,constant}(t)$ in Figs 14 and 15 are shown in Fig. 18 along with the best least square distributions in each case. The mean absolute error between the histograms and the normal distributions are 0.0278 and 0.0294, respectively. A Kolmogorov–Smirnov test [**42**] showed no statistically significant differences of each disturbance from normality. Similarly, a Kolmogorov–Smirnov test showed that the histogram distributions in Fig. 18 are also statistically similar with p-value < 0.015. This strong normal result is not surprising since no active grid was used to produce turbulence that can be non-Gaussian [**31**], and in a number of cases, turbulence can be considered to be approximately Gaussian [**43**].

In addition, the equivalent angles in Figs 14, 15, and 18 that represent the disturbance are predominantly around 10–20°, which is realistic on the rocket frame. The closeness of the identified distributions in Fig. 18 shows that slight variations in the method of identifying the intrinsic rocket parameters has no significant effect on the final identified extrinsic disturbance, further demonstrating the overall robustness of the approach.

3.5 Simulating model with external disturbance

Using the identified disturbance $u_{d,\theta}(t)$ and $u_{d,constant}(t)$ from equations (50) and (51), and the parameters in

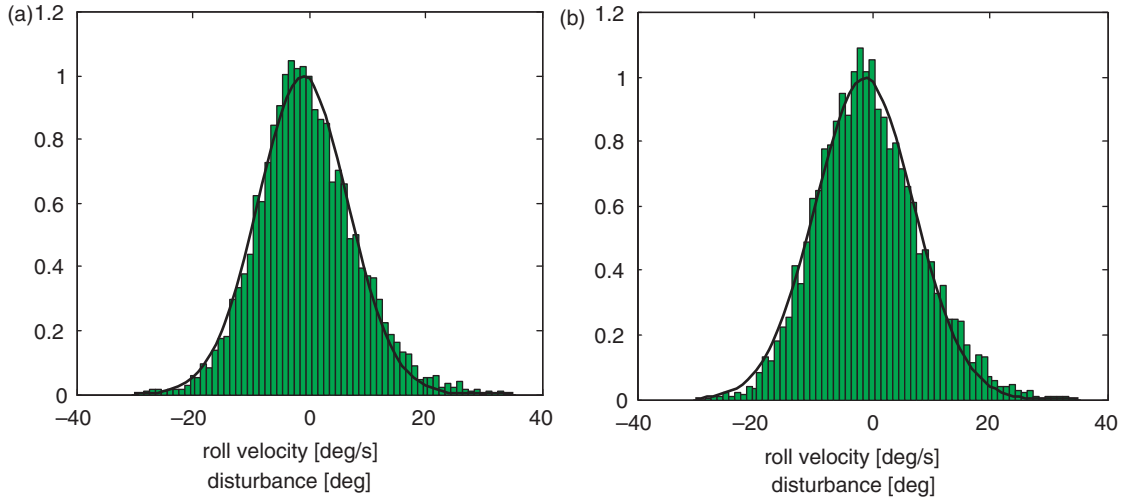

Fig. 18 Histograms of (a) disturbance $u_{d,\theta}(t)$ *vs* the best fitted normal distribution and (b) disturbance $u_{d,constant}(t)$ *vs* the best fitted normal distribution

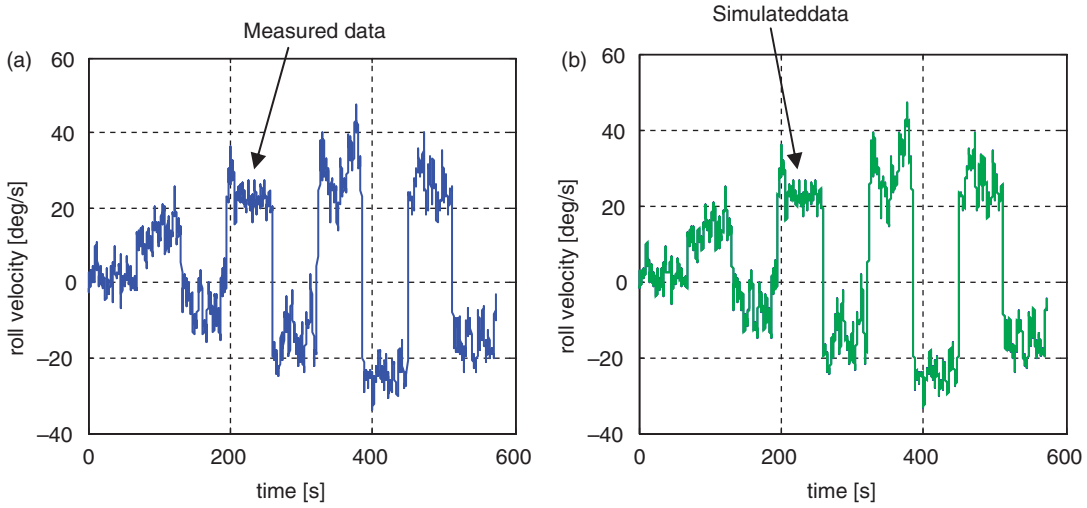

Fig. 19 (a) Angular velocity from experiment obtained by differentiating the measured encoder output. (b) Modelled output of angular velocity showing model based on θ-dependant damping coefficient (blue solid line) and constant damping coefficient (green dotted line)

equations (46) and (48), the models of equation (29) and (49) describing the full roll dynamics are numerically solved for the velocity and compared to the measured velocity in Fig. 19. In addition, the angular position of the rocket is found by integrating the modelled velocity and is compared to the measured angular position in Fig. 20. Both results show that the two models closely capture the actual data obtained from the experiment with each model output effectively overlaid. Specifically, the model of equation (29) with the constant damping parameter predicted the angular velocity with a mean absolute error of 0.094°/s and a standard deviation of 0.073°/s. The model tracked the roll angle (as measured by an encoder) with a mean absolute error of 0.13° and a standard deviation of 0.11°.

In comparison, the model of equation (49) with the θ-dependant damping parameter, allowing for changes in the inertia of the rocket, predicted the angular velocity with a mean absolute error of 0.097°/s and a standard deviation of 0.078°/s. This model tracked the roll angle with a median absolute error of 0.18° and a standard deviation of 0.14°.

The error between the modelled and measured roll angle is plotted in Fig. 21. Both models give similarly accurate results as expected, since any potential error in the intrinsic modelled parameters of the rocket would be 'lumped' into the disturbance profile.

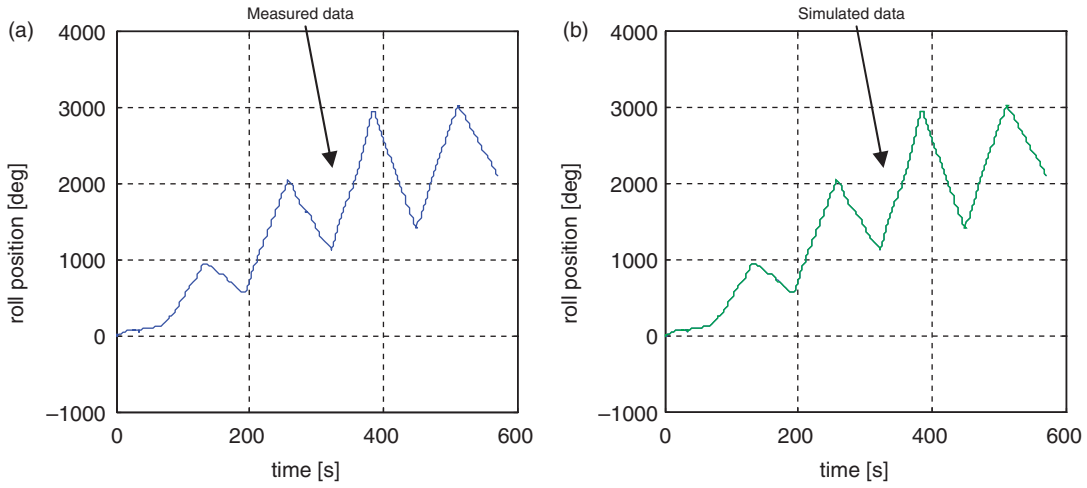

Fig. 20 (a) Angular displacement as measured from encoder. (b) Modelled output of angular displacement showing model based on θ-dependant damping coefficient (blue solid line) and constant damping coefficient (green dotted line)

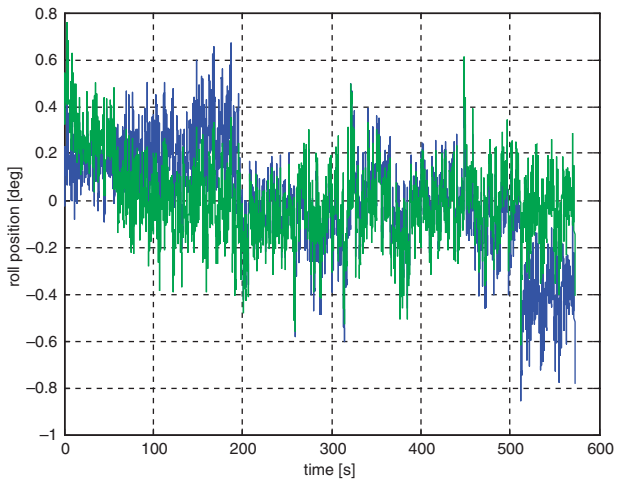

Fig. 21 Error between the modelled and recorded roll angle of the rocket frame for the θ-dependant damping coefficient (blue solid line) and constant damping coefficient (green dotted line)

4 LIMITATIONS AND FUTURE WORK

The current analysis has been restricted to the roll of the rocket. The actuation fins could be altered to provide pitch and yaw movements. A significant yaw movement will contribute a rolling moment to L in equation (4). Currently, the modelling approach would lump this yaw contribution as an external disturbance on the roll dynamics of equation (7). The same concept of separating intrinsic parameters from external random disturbances could, in principle, be applied to this case and to pitch movements using equations (1) to (3) and including the appropriate moments L, M, and N [**19**, **20**]. Furthermore, pitch and yaw movements could be included in a wind tunnel analysis [**44**].

However, roll dynamics alone without any pitch and yaw actuation inputs can have very complex non-linear behaviour and are still not fully understood [**45**]. Thus, they provide a good dynamic system to study the effects of random wind forcing during flight. Hence, the methods in this article are applicable to the development and testing of roll control only in rocket flights, but could be extended to pitch and yaw in the future.

The rocket roll data analysed in this article were performed for a single constant maximum fan speed. In practice, the velocity of the rocket increases significantly during thrust; so, the methods will only apply for a small portion or operating point of the flight. If the velocity increases, the dynamic pressure q in equation (5) will also increase, thus this situation is automatically handled by equations (1) to (5). Specifically, the current approach could be extended to this case by identifying the coefficient C_P in equation (8) instead of the lumped effect of c in equation (7). Rocket flight tests are needed to characterize the effectiveness of the modelling methodologies for this case and are left or future work. In addition, for speeds past approximately Mach 0.8, the coefficient C_P and moment coefficients in all axes can change significantly with respect to Mach number and angle of attack. A number of packages exist that characterize rocket aerodynamics up high Mach numbers and angles of attack [**46**, **47**]. Therefore, in principle, the methods in this article could be extended to these higher speeds and increased non-linearities.

The current wind tunnel setup was designed as an initial test of the developed modelling and system

identification methodologies. The standard reduction part, test section, wire mesh, and honeycomb flow straightener [**3**, **25**–**27**] were not considered in this first up test, as a good uniform air flow was not required. The main purpose was to test the ability of the developed algorithms to separate intrinsic parameters from external disturbances in a reasonably realistic case before the development of more sophisticated testing facilities in the future.

The wind speed of the wind tunnel was estimated to be roughly 50 km/h. However, a limitation of the current simplified wind tunnel setup of Fig. 1 is that it produces uncontrolled and very high velocity fluctuations, swirling, and turbulence, which are very difficult to measure and characterize accurately. The standard approach to simulating turbulence in a wind tunnel is by use of grids and bars based on an initial close to laminar flow, with very low turbulence. Different levels of turbulence intensity can then be investigated and the resulting wind speeds and variation measured in a controlled environment [**25**–**27**]. Future work will investigate these procedures.

5 CONCLUSION

A minimal modelling approach and integral-based parameter identification method were used to analyse roll dynamics of a sounding rocket airframe inside a vertical wind tunnel. By allowing a sufficient time to elapse after each step input, the disturbance was decoupled from the intrinsic dynamics of the rocket. This approach enabled an accurate calculation of the inertia and damping. Two cases of constant damping and time-varying damping were considered. For time-varying damping, the damping coefficient identified across each fin angle change was correlated with the absolute value of the effective fin angle which was a correction for asymmetries in the rocket. A very significant negative correlation was found which suggested the inertia of the rocket was increasing as the fin angle increased. Further tests need to be done to fully validate this result, but it proved the concept of using simplified models to bootstrap a more complex model to capture the observed data.

The disturbance profile was modelled by a sequence of effective fin angles that reproduce the velocity response as though the rocket was in a theoretically laminar flow. The overall outputs for both models closely matched the measured values for the roll rate and angle. This result demonstrates that the algorithms can be generalized to more detailed and physically accurate models. The identified disturbance profiles gave realistic magnitudes and close to normal distributions, providing further validation to the overall approach.

Future work includes investigating how other key variables such as rocket speed affects roll dynamics as well as extending the approach to pitch and yaw.

REFERENCES

1 **Eberspeaker, P. J.** and **Gregory, D. D.** An overview of the NASA sounding rockets and balloon programs. In Proceedings of the 18th Esa Symposium on *European rocket and balloon programmes and related research*, Visby, Sweden, 3–7 June 2007, vol. 647, pp. 25–32 (European Space Agency, Paris, France).

2 **Stamminger, A., Turner, J., Horschgen, M.,** and **Jung, W.** Sounding rockets as a real flight platform for aerothermodynamic CFD validation of hypersonic flight experiments. In Proceedings of the Fifth European Symposium on *Aerothermodynamics for space vehicles*, Cologne, Germany, 8–11 November 2004, vol. 563, pp. 431–437.

3 **Schrijer, F.** and **Bannink, W.** Description and flow assessment of the delft hypersonic ludwieg tube. *J. Spacecr. Rockets*, 2010, **47**, 125–133.

4 **Saravanan, S., Nagashetty, K., Hegde, G., Jagadeesh, G.,** and **Reddy, K.** Schlieren visualization of shock wave phenomena over a missile-shaped body at hypersonic Mach numbers. *Proc. IMechE, Part G: J. Aerospace Engineering*, 2011, **225**, 26–34.

5 University of Canterbury. UC Rocketry Project, 2011, available from http://www.ucrocketry.com/ (access date 17 March 2011)

6 **Hann, C., Singh-Levett, I., Deam, B., Mander, J.,** and **Chase, J.** Real-time system identification of a nonlinear four-story steel frame structure—application to structural health monitoring. *IEEE Sens. J.*, 2009, **9**, 1339–1346.

7 **Hann, C., Sirisena, H.,** and **Wongvanich, N.** Simplified modeling approach to system identification of nonlinear boat dynamics. In Proceedings of the 2010 American Control Conference (ACC2010), Baltimore, Maryland, USA, June 30 to July 2 2010, pp. 5218–5223 (IEEE, Piscataway, New Jersey).

8 **Hann, C. E., Aitchison, D., Kirk, D.,** and **Brouwers, E.** Modelling and system identification of a stiff stay wire fence machine. *Proc. IMechE, Part G: J. Aerospace Engineering*, 2010, **224**, 1069–1083.

9 **Shaw, G. M., Chase, J. G., Starfinger, C., Smith, B. W., Hann, C. E., Desaive, T.,** and **Ghuysen, A.** Modelling the cardiovascular system. *Crit Care Resusc.*, 2007, **9**, 263–269.

10 **Cochran, J. E.** and **Beaty, J. R.** Simulation of the flight of a short range air defense system rocket before radar acquisition, Technical Report, Auburn University, 1977.

11 **Moore, F. G.** and **Moore, L. Y.** New method to predict nonlinear roll damping moments. *J. Spacecr. Rockets*, 2008, **45**, 955–964.

12 **Moore, F. G.** and **Moore, L. Y.** New methods to predict nonlinear pitch damping moments. *J. Spacecr. Rockets*, 2008, **45**, 495–503.

13 **Moore, F. G., McInville, R. M.,** and **Hymer, T. C.** Evaluation and improvements to the aeroprediction code based on recent test data. *J. Spacecr. Rockets*, 2000, **37**, 720–730.

14 **Peters, J.** and **Schaal, S.** Learning to control in operational space. *Int. J. Rob. Res.*, 2008, **27**, 197–212.

15 **Vachtsevanos, G., Tang, L., Drozeski, G.,** and **Gutierrez, L.** From mission planning to flight control of unmanned aerial vehicles: strategies and implementation tools. *Annu. Rev. Control*, 2005, **29**, 101–115.

16 **Liang, W.** and **Song, F.** Modelling flow transition in a hypersonic boundary layer with Reynolds-averaged Navier-Stokes approach. *Sci. Chin. Ser. G-Phys. Mech. Astron.*, 2009, **52**, 768–774.

17 **Longo, J. M. A.** Modelling of hypersonic flow phenomena. In Proceedings of the Critical Technologies for Hypersonic Vehicle Development Technology, Rhode Saint Genèse, Belgium, 1–2 April 2004, VKI-RTO Lecture Series, pp. 1–26.

18 **Pattinson, J., Malan, A.,** and **Meyer, J.** A cut cell non conforming Cartesian mesh method for compressible and incompressible flow. *Int. J. Numer. Methods Engng*, 2007, **72**, 1332–1354.

19 **Siouris, G. M.** *Missile guidance and control systems*, 2004 (Springer Verlag, New York).

20 **Tewari, A.** *Atmospheric and space flight dynamics: modeling and simulation with MATLAB and Simulink*, 2007 (Springer, New York).

21 **Lazic, D. V.** and **Ristanovic, M. R.** Electrohydraulic thrust vector control of twin rocket engines with position feedback via angular transducers. *Control Engng Pract.*, 2007, **15**, 583–594.

22 **Lee, H. I., Sun, B. C., Tahk, M. J.,** and **Lee, H.** Control design of spinning rockets based on co-evolutionary optimization. *Control Engng Pract.*, 2001, **9**, 149–157.

23 **Dehghan Manshadi, M., Mirzaei, M., Soltani, M.,** and **Ghorbanian, K.** Control of pressure gradient in the contraction of a wind tunnel. *World Acad. Sci. Engng Technol.*, 2008, **40**, 261–266.

24 **Timmer, W.** Two-dimensional low-Reynolds number wind tunnel results for airfoil NACA 0018. *Wind Engng*, 2008, **32**, 525–537.

25 **Pennycuick, C.** and **Alerstam, T.** A new low-turbulence wind tunnel for bird flight experiments at Lund University, Sweden. *J. Exp. Biol.*, 1997, **200**, 1441–1449.

26 **Mehta, R. D.** Turbulent boundary-layer perturbed by a screen. *AIAA J.*, 1985, **23**, 1335–1342.

27 **Scheiman, J.** and **Brooks, J. D.** Comparison of experimental and theoretical turbulence reduction from screens, honeycomb, and honeycomb-screen combinations. *J. Aircr.*, 1981, **18**, 638–643.

28 **Goes, L. C., Hemerly, E. M., Maciel, B. C. D., Neto, W. R., Mendonca, C. B.,** and **Hoff, J.** Aircraft parameter estimation using output-error methods. *Inverse Prob. Sci. Engng*, 2006, **14**, 651–664.

29 **Jategaonkar, R.** and **Thielecke, F.** ESTIMA - an integrated software tool for nonlinear parameter estimation. *Aerosp. Sci. Technol.*, 2002, **6**, 565–578.

30 **GarciaVelo, J.** and **Walker, B. K.** Aerodynamic parameter estimation for high-performance aircraft using extended Kalman filtering. *J. Guid. Control Dyn.*, 1997, **20**, 1257–1259.

31 **Makita, H.** Realization of a large-scale turbulence field in a small wind tunnel. *Fluid Dyn. Res.*, 1991, **8**, 53–64.

32 **Shenzhen Secom Telecom Co., Ltd.** Available from http://www.secomtel.com/UpFilesPDF/PDF/Agilent/PDF_DOCS/ISONCONT/02_MOTN/2_116_18.pdf (access date 19 August 2011).

33 **Liu, X., Xiao, L., He, X.,** and **Xu, J.** Signal reconfiguration of missile fault-tolerant control. *Proc. IMechE, Part G: J. Aerospace Engineering*, 2006, **220**, 429–437.

34 **Jahnke, C. C.** On the roll–coupling instabilities of high–performance aircraft. *Philos. Trans. R. Soc. Lond., Ser. A*, 1998, **356**, 2223.

35 **Day, R. E.** *Coupling dynamics in aircraft: a historical perspective*, NASA publication no. SP-532, 1997 (Citeseer, NASA Dryden Flight Research Center, Edwards, California).

36 **Hull, D. G. Ontario IfCESi.** *Fundamentals of airplane flight mechanics*, 2007 (Springer, Berlin).

37 **Hann, C. E., Chase, J. G., Lin, J., Lotz, T., Doran, C. V.,** and **Shaw, G. M.** Integral-based parameter identification for long-term dynamic verification of a glucose-insulin system model. *Comput. Methods Progr Biomed.*, 2005, **77**, 259–270.

38 **Hann, C. E., Chase, J. G., Ypma, M. F., Elfring, J., Nor, N. M., Lawrence, P.,** and **Shaw, G. M.** The impact of parameter identification methods on drug therapy control in an intensive care unit. *Open Med. Inform. J.*, 2008, **2**, 92–104.

39 **Roy, C.** and **Blottner, F.** Assessment of one-and two-equation turbulence models for hypersonic transitional flows. *J. Spacecr. Rockets*, 2001, **38**, 699–710.

40 **Zhuravlev, V.** Turbulence of incompressible liquid flows near local equilibrium and the secondary entropy maximum principle. *Tech. Phys.*, 2010, **55**, 654–665.

41 **Perez, T.** and **Fossen, T.** Joint identification of infinite-frequency added mass and fluid-memory models of marine structures. *Model. Ident. Control*, 2008, **29**, 93–102.

42 **Lilliefors, H.** On the Kolmogorov-Smirnov test for normality with mean and variance unknown. *J. Am. Stat. Assoc.*, 1967, **62**, 399–402.

43 **Aringazin, A.** and **Mazhitov, M.** The PDF of fluid particle acceleration in turbulent flow with underlying normal distribution of velocity fluctuations. *Phys. Lett. A*, 2003, **313**, 284–290.

44 **Magill, C., Cataldi, P., Morency, J., Burgess, R., Daugherty, C.,** and **Jeter, E.** Demonstration of a wire suspension for virtual flight testing in a wind tunnel. *AIAA J. Spacecr. Rockets*, 2009, **46**(3), 624–633.

45 **Moore, F.** and **Moore, L.** New method to predict nonlinear roll damping moments. *J. Spacecr. Rockets*, 2008, **45**, 955–964.

46 Sooy, T. J. and **Schmidt, R. Z.** Aerodynamic predictions, comparisons, and validations using MISSILE DATCOM (97) and aeroprediction 98 (AP98). *J. Spacecr. Rockets*, 2005, **42**, 257–265.

47 Abney, E. and **McDaniel, M. A.** High angle of attack aerodynamic predictions using missile DATCOM. In Proceedings of 23rd AIAA Applied Aerodynamics Conference, AIAA paper no. 2005-5086, Toronto, Ontario Canada, 6–9 June 2005, 19p. (American Institute of Aeronautics and Astronautics, Reston, Virginia).

APPENDIX

Notation

a	generic damping parameter including inertia
$a(t), a_i$	piecewise constant time-varying parameter with constants a_i
$a_i,\ b_i$	parameters defining $\theta_{model}(t)$
$\boldsymbol{A}, \boldsymbol{B}$	matrices describing the equation for determining the parameters of $\theta_{model}(t)$
b	generic torque constant
b	lumped parameter torque constant
c	lumped parameter damping coefficient
$c.g.$	centre of gravity
C	matrix in the equation determining the parameters a_i from the measured roll velocity data
$\bar{\boldsymbol{C}}_i, \bar{\boldsymbol{D}}_i$	vectors describing the equation for determining the unknown disturbance constants $u_{\mathrm{d},i}$ from the measured roll velocity data
C_P	variation of rolling moment coefficient with dimensionless rate of change of roll rate
C_R	variation of rolling moment coefficient with dimensionless rate of change of yaw rate
C_β	variation of rolling moment coefficient with angle of slide slip
$C_{\dot{\beta}}$	variation of rolling moment coefficient with dimensionless rate of change of angle of sideslip
C_δ	variation of rolling moment coefficient with fin angle.
d	maximum diameter of rocket body
$f_{ext}(\theta)$	external torque resulting from a change in the fin angle θ
f_{ss}	steady-state fin angle deflection
$H(t)$	Heaviside function
I	shortened notation of I_{xx}
$\boldsymbol{I}_{N_i}, \bar{\boldsymbol{v}}_{data,\,N_i}$	vectors of each step response time interval describing the equation for determining the generic damping parameter a from the roll velocity data
I_{xx}	rotation inertia about X_b axis
I_{yy}	rotation inertia about Y_b axis
I_{zz}	rotation inertia about Z_b axis
L	moment about the X_b axis
M	moment about the Y_b axis
N	moment about the Z_b axis
$\bar{N}$	total number of time points in T_{vector}
N_i	number of time points in each ith segment $t \in [T_i, T_{i+1}]$
N_t	number of time points for each sampling period
N_{total}	total number of time intervals Δt that fit in the whole time period
P	yaw angle aboutX_b axis
Q	yaw angle about Y_b axis
R	yaw angle about Z_b axis
S	maximum cross-sectional area of rocket body
t_{lag}	time lag in servo-motor for the fin actuation
$\bar{t}_{vector}$	vector of all sampled time points
t_0	break point of bi-linear model
T_i	time of ith step in $\theta_{model}(t)$
$\bar{T}_{N_{i\times 2}}, \underline{O}_{m\times n}$	matrices determining A, B
T_{vector}	vector of time points containing all segments
$u_{\mathrm{d},i}$	unknown constant across each time interval of length Δt
$\bar{u}_{\mathrm{d},i}$	lumped unknown parameter $=a_i u_{\mathrm{d},i}$
$u_d(t)$	unknown, time-varying and piecewise constant disturbance model due to turbulence in the wind tunnel
$u_{\mathrm{d},\theta}(t)$	identified disturbance based on θ-dependent damping coefficient
$U_{\mathrm{d},constant}(t)$	identified disturbance based on constant damping coefficient
v	equivalent notation for the roll velocity p
$\bar{v}_{data}$	vector containing all the roll velocity data from each time interval
v_{model}	bi-linear model for the roll step response
v_M	magnitude of the velocity of the centre of mass
v_{ss}	steady-state roll rate
$v_{ss,new}$	linear model describing relationship between f_{ss} and v_{ss}
v_0	initial velocity in step response
α, β	parameters in the model $v_{ss,new}$
β	slide slip angle
δ	fin actuation angle

δt	sampling period for interpolating the data (at 100 Hz)
Δt	time interval defining piecewise constant function $u_d(t)$
ΔT_0	time interval bounding break point of bi-linear model
ε	random number sampled from normal distribution
η	noise percentage for simulating measurement error in roll velocity
θ	equivalent notation for the fin actuation angle δ
$\bar{\theta}$	off-set angle describing the asymmetry of model
$\theta_{data}(t)$	measured encoder data for the roll angle θ
$\theta_{effective}$	effective fin angle causing a roll due to asymmetry in rocket
$\theta_{model}(t)$	piecewise linear model of the roll angle θ
θ_{ss}	steady-state roll angle after a fin movement
μ, σ	mean and standard deviation of a normal distribution
ρ	air density
$\tau_d(t)$	external disturbance torque affecting roll